Localized Surface Plasmon Resonances Arising from Free Carriers in Doped Quantum Dots

Joseph M. Luther,[1,2,†] Prashant K. Jain,[1,2,3,†] Trevor Ewers,[1,2] and A. Paul Alivisatos[1,2,*]
[1]*Department of Chemistry, University of California, Berkeley CA 94720*
[2]*Materials Sciences Division, Lawrence Berkeley National Laboratory, Berkeley CA 947203*
[3]*Miller Institute for Basic Research in Science, University of California, Berkeley CA 94720*
[†]*these authors contributed equally*
**Corresponding Author E-mail: apalivisatos@lbl.gov*

Localized surface plasmon resonances (LSPRs) typically arise in nanostructures of noble metals[1, 2] resulting in enhanced and geometrically tunable absorption and scattering resonances. LSPRs however are not limited to nanostructures of metals and can also be achieved in semiconductor nanocrystals with appreciable free carrier concentrations. Here, we describe well-defined LSPRs arising from *p*-type carriers in vacancy-doped semiconductor quantum dots (QDs). Achievement of LSPRs by free carrier doping of a semiconductor nanocrystal would allow active control of LSPR response *on chip*. Plasmonic sensing and manipulation of solid-state processes in single nanocrystals constitutes another interesting possibility. We also demonstrate that doped semiconductor QDs allow realization of LSPRs and quantum-confined excitons within the same nanostructure opening up the possibility of strong coupling of photonic and electronic modes, with implications for light harvesting, non-linear optics, and quantum information processing.

The interaction of nanoscale metals with light is characterized by surface-bound charge density oscillations of their free electrons in resonance with the driving electromagnetic field. On account of these so called localized surface plasmon resonances (LSPRs), the nanoparticles show intense light absorption and scattering with potential uses in many fields ranging from photovoltaics[3] to bio-imaging and laser photothermal therapy.[2] At resonance, the electric field at the surface of the nanoparticle is strongly enhanced, resulting in molecules in the vicinity exhibiting enhanced absorption and emission, Raman scattering, and non-linear optical properties.[4] The strongly confined LSPR near-field is used in sub-wavelength microscopy, near-field lithography,

nanophotonics,[1] and as a single-molecule detection probe of the local medium surrounding the nanostructure.[5]

The LSPR frequency, while somewhat tunable by the nanostructure size, geometry, and local medium, is primarily controlled through the free electron density (*N*) of the material modulated by its high frequency dielectric constant (ε_∞).[6, 7] The most common plasmonic metals, viz., gold, silver, and copper have free electron densities in the range 10^{22}-10^{23} cm^{-3} with corresponding LSPRs in the visible.[6] Plasmon resonances are not however fundamentally limited to metals and occur in conducting metal oxides[8] as well as in semiconductors with appreciable free carrier densities. While free carrier absorption and plasmon resonances have been studied in doped semiconductor films, LSPRs have not been investigated in semiconductor nanocrystals. In principle, semiconductor nanostructures are expected to display similar size- and shape-tunability of LSPRs as metals. However, a key advantage of using semiconductors for nanoplasmonics is that their free carrier concentrations can be tuned by doping, temperature, and/or phase transitions, allowing not only the engineering of LSPRs, but also their active control or switching within a working device (for instance, via electrochemical charge injection, gating, or temperature control). The LSPR response of a metal nanoparticle, on the other hand, once engineered by choice of nanostructure parameters, such as shape, size, or metal, is permanently locked-in and cannot be dynamically controlled.

Fig 1 depicts the LSPR tunability (either static or dynamic) achievable by controlled doping of semiconductor nanocrystals. Typical doping concentrations (10^{16}-10^{19} cm^{-3}) would result in LSPRs in the THz regime with possible applications in THz imaging and nanophotonic circuitry.[9] Carrier concentrations of ~10^{21} cm^{-3} would result in LSPRs in the near- or mid-infrared (NIR or MIR), allowing for a range of applications including near-field IR imaging and lithography with $\lambda/100$ resolution, plasmon-enhanced absorption for photon harvesting in the red end of the solar spectrum, and surface-enhanced infrared absorption (SEIRA) spectroscopy of molecules.[10] However, efforts to intentionally dope

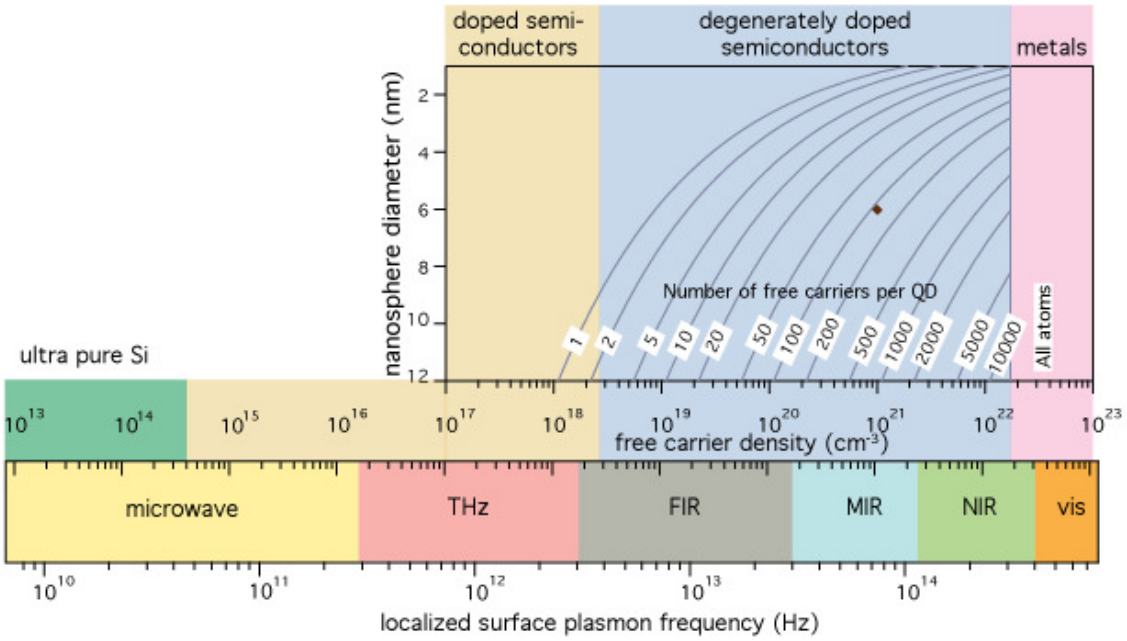

Figure 1. Localized surface plasmon resonance (LSPR) frequency dependence on free carrier density and doping constraints. The bottom panel shows the modulation of the LSPR frequency (ν_{sp}) of a spherical nanoparticle by control of its free carrier concentration (N). LSPR frequency is estimated as: $\frac{1}{2\pi}\sqrt{\frac{Ne^2}{\varepsilon_0 m_e(\varepsilon_\infty+2\varepsilon_m)}}$. The high frequency dielectric constant ε_∞ is assumed to be 10, the medium dielectric constant ε_m is set as 2.25 for toluene, and the effective mass of the free carrier m_e is assumed to be that of a free electron. e is the electronic charge and ε_o is the permittivity of free space. The top panel shows a calculation of the number of dopant atoms required for nanoparticle sizes ranging from 2 to 12 nm to achieve a free carrier density between 10^{17} and 10^{23} cm^{-3}. To achieve LSPRs in the visible region, a material in which every atom contributes a free carrier to the nanoparticle, i.e. a metal, is required. For LSPRs in the infra-red, carrier densities of 10^{19}-10^{22} cm^{-3} are required. Below 10^{19} cm^{-3}, the number of carriers (for a 10-nm nanocrystal) may be too low (<10) to support an LSPR mode. The brown diamond indicates the region of interest in the present study.

colloidal nanocrystals, as commonly done in bulk semiconductors, have been met with limited success as self-purification of the crystal during growth expels dopant atoms to the surface.[11] Consequently, only equivalent-valency ions are normally incorporated, leading to no ionized free carriers for achieving LSPRs.

Here, we demonstrate strong NIR LSPRs in quantum dots (QDs) of the semiconductor copper (I) sulfide. $Cu_{2-x}S$ can support numerous copper-deficient stoichiometries[12] and as a result is highly self doped (*p*-type). $Cu_{2-x}S$ has been synthesized[13-17] and explored for optoelectronic applications due to its near-ideal band-gap for photovoltaics and high earth abundancy.[18] Stoichiometry-dependent NIR absorption of nanosized $Cu_{2-x}S$ has also been investigated.[19] Figure 2 shows TEM

images, electron diffraction patterns, and size histograms of $Cu_{2-x}S$ QDs of good monodispersity with average diameters ranging from 2-6 nm. We discuss the optical properties which show quantum-confined excitonic as well as LSPR bands. The LSPR corresponds to a vacancy density of ~10^{21} cm^{-3} or a stoichiometry of $Cu_{1.93}S$, which is consistent with a common copper deficient phase known as djurleite,[20, 21] further supported by electron and X-ray diffraction (Fig. 2). This study opens up the possibility that other self-doped semiconductor QD systems such as GeTe or SnTe [22] support strong LSPRs.

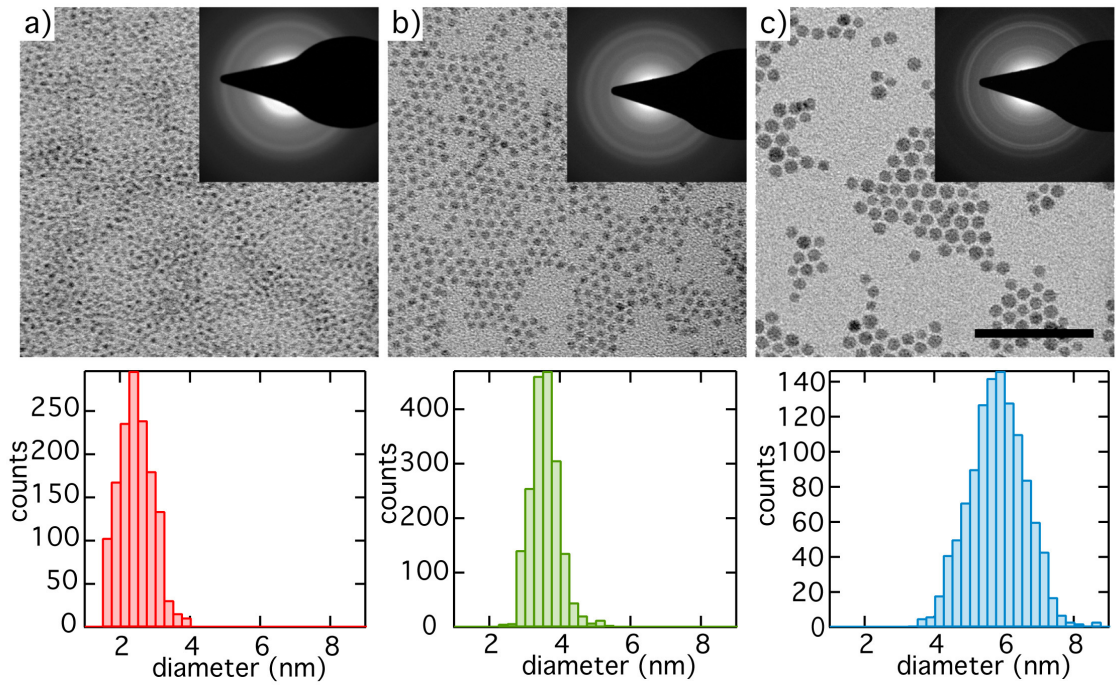

Figure 2. **Size-controlled synthesis of copper (I) sulfide QDs.** Transmission electron micrographs and (inset) electron diffraction patterns (top), and size distribution histograms (bottom) of three QD samples with average size of a) 2.4 $\pm$ 0.5 nm b) 3.6 $\pm$ 0.5 nm, and c) 5.8 $\pm$ 0.8 nm. Diffraction rings in inset of c) can be identified at d = 1.28, 1.70, 1.89, 1.98, 2.22, 2.41, 3.05, and 3.37 A^{o}.

The bulk bandgap of $Cu_{2-x}S$ is characterized by an absorption onset at 1.1-1.4 eV, depending on stoichiometry.[23] Figure 3a shows the absorbance for a series of the $Cu_{2-x}S$ QDs. Semiconducting QDs typically show a set of absorbance peaks attributable to quantum-confined excitons with the lowest energy peak

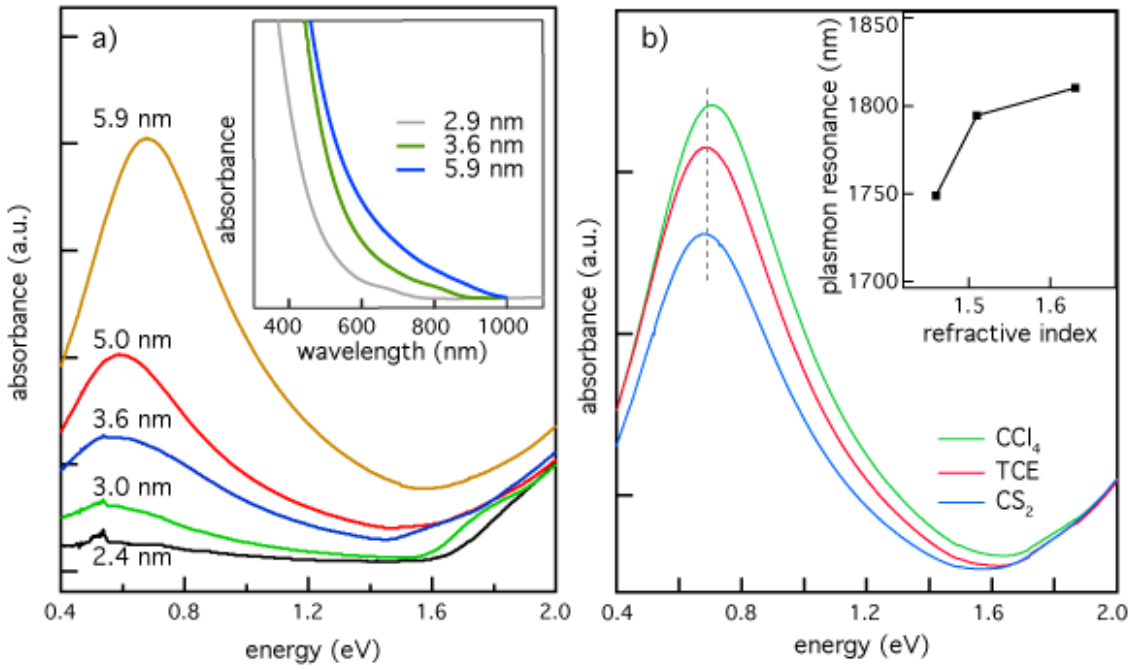

Figure 3. Excitons and localized surface plasmon resonances in absorbance spectra of $Cu_{2-x}S$ quantum dots. a) Size-dependent band-gap, excitonic, and LSPR absorption of copper sulfide QDs for representative sizes ranging from 2 to 6 nm. For the smallest QDs, the excitonic peak extends up to 1.8 eV, i.e., 0.5 eV blue-shift relative to the bulk band gap. The inset shows the excitonic structure on wavelength scale. Near-infrared (NIR) absorption for copper (I) sulfide QDs of different sizes dispersed in tetrachloroethylene (TCE) show clear LSPRs. With decreasing size of the QDs in, the LSPR band broadens and progressively red-shifts. The plasmon resonance is completely damped for the sub-3-nm QDs. This trend, similar to that observed by Whetten and coworkers in small gold nanocrystals, can be attributed to the effect of surface scattering of free carriers (see Supplementary Information).[6] b) 6-nm QDs dispersed in three different solvents: carbon tetrachloride, TCE, and carbon disulfide with refractive indices of 1.46, 1.51, and 1.63, respectively. The inset shows the red-shift in the LSPR maximum with increasing solvent refractive index. The LSPR frequency and line-width were determined by fitting the NIR absorption band to a Gaussian function. From the inset, the LSPR sensitivity is estimated to be ~350 nm/RIU, which is somewhat higher than the values for silver nanotriangle arrays that are commonly used for LSPR sensing. When normalized by the LSPR linewidth, we obtain a modest sensing figure of merit of ~0.7 in the NIR.

corresponding to the $1S_h$-$1S_e$ excitonic transition (the quantized band-gap), which blue-shifts with decreasing QD size.[24] $Cu_{2-x}S$ nanocrystals (Fig. 3a inset) clearly show broad excitonic peaks, which blue-shift from bulk with decreasing QD size, the onset ranging from 1.3-1.6 eV. Exciton features in copper sulfide nanoparticles have only been observed previously for relatively monodisperse nanorods made indirectly from the Cu^+ exchange of CdS.[25] The size-dependent band gaps observed are consistent with estimations of a Bohr radius of 3-5 nm for $Cu_{2-x}S$ and prediction of strong confinement effects below 10 nm.[19]

Bulk $Cu_{2-x}S$ shows a free-carrier absorption in the NIR region from excess holes in the valance band due to copper deficiencies.[26] In bulk, no absorption is seen for perfectly stoichiometric Cu_2S, and the free carrier absorption intensity increases with x.[26] Nanocrystallites of $Cu_{2-x}S$ exhibit a similar trend in their NIR absorption as a function of stoichiometry as that in the bulk.[19] The free-carrier absorption region in our case is distinguished by remarkably well-defined peaks (Figure 3), characteristic of LSPR modes, the free carriers being holes, rather than electrons as in the case of metals.[2] We believe that the relatively high monodispersity and lack of inter-particle aggregation result in our colloids exhibiting sharp plasmon absorption peaks.

Sub-bandgap absorption can arise from other phenomena such as scattering or sample impurities, but we can assign the NIR absorption bands to LSPRs by studying the effect of the solvent medium on the absorption band position.[2] We compared NIR spectra of the QDs in three different solvents: CCl_4, TCE, and CS_2 with refractive indices of 1.46, 1.51, and 1.63, respectively (Fig. 3b). The NIR absorption band red-shifts with increasing refractive index, as expected from an LSPR feature. The magnitude of spectral shift is complicated since the ligand shell contributes to the effective local medium index.

The resonance wavelength correlates with the excess free carrier density in the QDs. From past studies on noble metal nanoparticles, the LSPR frequency is determined by the complex dielectric function, ε, of the plasmonic material, the size, shape, and dielectric constant, ε_m, of the environment of the nanoparticle.[2] The dipole polarizability, α, of a small spherical nanoparticle with size much smaller than the wavelength of the light is given as:

$$\alpha = 3\varepsilon_0 V \frac{(\varepsilon-\varepsilon_m)}{(\varepsilon+2\varepsilon_m)} \qquad (1)$$

where V is the nanoparticle volume and ε_0 is free space permittivity. Such a nanoparticle displays a dipolar LSPR when the denominator diminishes, i.e. when:

$$\varepsilon_r = -2\varepsilon_m \qquad (2)$$

where ε_r denotes the real part of ε, expressed as a function of the frequency of light, ω, by the Drude model:

$$\varepsilon_r = 1 - \frac{\omega_p^2}{\omega^2+\gamma^2} \qquad (3)$$

Here ω_p is the bulk plasma oscillation frequency associated with the free carriers and γ is their bulk collision frequency. From (2) and (3) we get the frequency ω_{sp} at which the resonance condition described by Eq. 2 is satisfied:

$$\omega_{sp} = \sqrt{\frac{\omega_p^2}{1+2\varepsilon_m} - \gamma^2} \quad (4)$$

ω_{sp} represents the LSPR energy and γ represents the linewidth of the plasmon resonance band. From Fig. 3a, the LSPR band of the 6-nm QDs in TCE ($\varepsilon_m = 2.28$) shows a resonance energy ω_{sp} of 0.69 eV and a linewidth γ of 0.21 eV. Thus, from Eq. 4 we estimate the plasma frequency ω_p of the free carriers in copper sulfide as 1.7 eV. We assume that the dielectric function of copper sulfide in the NIR region is dominated by free carriers, since the band-gap contribution can be neglected.

The bulk plasma frequency ω_p depends on the density N_h of free carriers (holes) as:

$$\omega_p = \sqrt{\frac{N_h e^2}{\varepsilon_0 m_h}} \quad (5)$$

where m_h is the hole effective mass, approximated as $0.8m_o$ where m_o is the electron mass.[19] From Eq. 5, N_h is estimated to be 1.7 x 10^{21} cm^{-3}. Comparatively, N_e in gold is 5.9 x 10^{22} cm^{-3}. The quality factor of an LSPR mode is defined by the ratio of the resonance peak energy to the peak linewidth (disregarding inhomogeneous broadening). The quality factor here is ~3 on par with that for gold nanoparticles (~9 as per a theoretical Mie extinction spectrum of a 10-nm colloid in water). The LSPR peak extinction cross-section of the 6-nm nanocrystals is estimated using the Clausius-Mossotti polarizability to be 8 nm^2, amounting to a molar extinction coefficient of 2 x 10^7 M^{-1} cm^{-1}.

Hole densities of 10^{21} cm^{-3} are typical in copper chalcogenide films.[26] From the calculated N_h, we estimate ~200 excess holes per 6-nm QD, which is reasonable enough to support a particle plasmon resonance. The LSPR serves to profile the stoichiometric state of the nanocrystal lattice. Assuming each excess hole originates from one copper vacancy, we estimate a copper deficiency of 3.8%, i.e., a composition of $Cu_{1.93}S$. N_h is somewhat over-estimated because the experimental LSPR linewidth used in eq. 4 includes, in addition to the intrinsic broadening γ, the inhomogeneous broadening due to dispersion in nanocrystal size and vacancy density.

Copper (I) sulfide's varied crystallographic phases are based on a hexagonal close packing of the sulfur atoms.[21] The stable phase above 104°C is high chalcocite, in which case the copper atoms are virtually "fluid", resulting in a hexagonal crystallography defined by the sulfur framework. Below 104°C, the copper atoms pack in a complex interstitial manner, giving rise to a lower symmetry monoclinic phase, i.e low chalcocite.[20] While low chalcocite has a near-stoichiometric composition ($Cu_{1.997-2.0}S$), copper (I) sulfide has a thermodynamic propensity towards copper deficiency due to the low chemical potential of Cu^0.[27,28] Vacancies can form by the loss of copper to carbon dioxide or oxygen at a free surface or grain boundary:[21] processes likely enhanced at the nanoscale. Due to high ionic mobility, vacancies can cluster together in groups of four per $Cu_{20}S_{12}$ unit, with the remainder of the copper ordered similar to low chalcocite.[12, 20, 21] Djurleite, has a lower free energy than low chalcocite at room temperature due to its lower crystallographic symmetry, and thus is more stable in bulk[21,27] and in nanoparticles.[19] In fact, djurleite has been mistaken for chalcocite.[20] Transformation from low chalcocite to djurleite is facilitated by heat, electron beam, electric fields, or oxygen.[27]

Based on the known phase behavior of copper (I) sulfide, our high temperature synthesis most likely forms the high chalcocite phase, which on cooling stabilizes to the low chalcocite and/or copper-deficient djurleite, with a greater propensity for the latter.[27] A recent $Cu_{2-x}S$ nanocrystal synthesis at similar temperature reported the presence of djurleite.[17] X-ray diffraction (XRD) patterns of our samples suggest presence of low chalcocite or djurleite (SI) but XRD is known to be inconclusive for copper (I) sulfide.[19, 29] Electron diffraction (Fig. 2c inset and SI) shows a diffraction ring at d = 3.41 A°, within 1% of the diagnostic reflection (d = 3.39 A°)[29] of djurleite that is absent in low chalcocite, confirming the presence of djurleite.

Djurleite has a copper deficiency of 3.1%, in close agreement with the estimate of 3.8% from the plasmon resonance energy position. We expect some degree of imprecision in the LSPR estimate due to uncertainty of the hole effective mass, the Drude approximation, and the assumption that all copper vacancies are ionized, but it serves as a more reasonable estimate than conventional elemental analysis by energy dispersive X-ray analysis or inductively coupled plasma mass spectrometry. Inherent errors in these

measurements coupled with contribution of the surface atoms in small nanocrystals disallow reliable detection of 3% copper deficiency.

Stoichiometric composition and resulting vacancy densities of $Cu_{2-x}S$ nanocrystals can vary with conditions used for their synthesis and/or aging.[19] For instance, copper (I) sulfide nanorods made via the cation exchange of CdS nanorods at room temperature[25] are low chalcocite and lack LSPRs unlike the heavily self-doped nanocrystals synthesized in this study. In addition to synthetic variability, copper chalcogenide nanocrystals can undergo changes in composition and vacancy density over time from thermal aging, oxidation, or field-assisted copper migration, modifying critical optoelectronic properties. [27] In the absence of reliable analytical tools, LSPR spectroscopy can be used to profile the stoichiometry, phase, or vacancy density of such doped nanocrystals. The use of sensitive dark-field plasmon scattering microscopy opens up the possibility of probing compositional phase transitions or metal-to-insulator transitions in single QDs. The large plasmon absorption cross-section may allow optical switching of phases photothermally in single QDs.

Closely related materials like copper selenide have a similar tendency for copper-deficient compositions, both in bulk and nanocrystal form. Analysis of previously published absorbance spectra [30, 31] showed strong NIR bands characteristic of LSPR absorption. $Cu_{2-x}Se$ nanoparticles synthesized by Gurin et al. displayed bands in the 1000-1500 nm region, that were stoichiometry dependent; however these were tentatively assigned to impurity-level transitions, rather than LSPRs.[30] $Cu_{2-x}Se$ nanoparticles synthesized by Manna and coworkers exhibited an NIR band at 1150 nm.[31] From the plasmon resonance energy position (~1 eV), linewidth (~0.4 eV), effective mass (m_h ~ $0.4m_o$) and high- frequency dielectric constant (ε_∞ ~ 7),[32] we can assign this band to an LSPR with hole density estimated to be ~4 x 10^{21} cm^{-3}, similar to values for $Cu_{2-x}Se$ films with x = 0.1-0.2,[32] and consistent with their measured resistivity of ~6 x 10^{-3} Ω cm.[31] From the plasmon resonance analysis, we estimate the nanocrystal composition to be $Cu_{1.8}Se$, in agreement with the range ($Cu_{1.7}Se$ to $Cu_{1.9}Se$) measured by the authors.[31]

Since doping allows the modulation of electronic, optical, and magnetic properties of semiconductors nanocrystals, the high self-doping in copper chalcogenide nanocrystals is fundamentally interesting. The ability to reliably control and characterize vacancy

densities in these nanocrystals and those of similarly self-doped nanocrystals is worth exploring from the point of view of active tuning of nanoplasmonic responses. As a demonstration, we synthesized Cu_2S nanocrystals with minimal copper vacancies by room temperature cation exchange of CdS nanorods, a method that is proposed to result in nearly stoichiometric low chalcocite phase.[33]

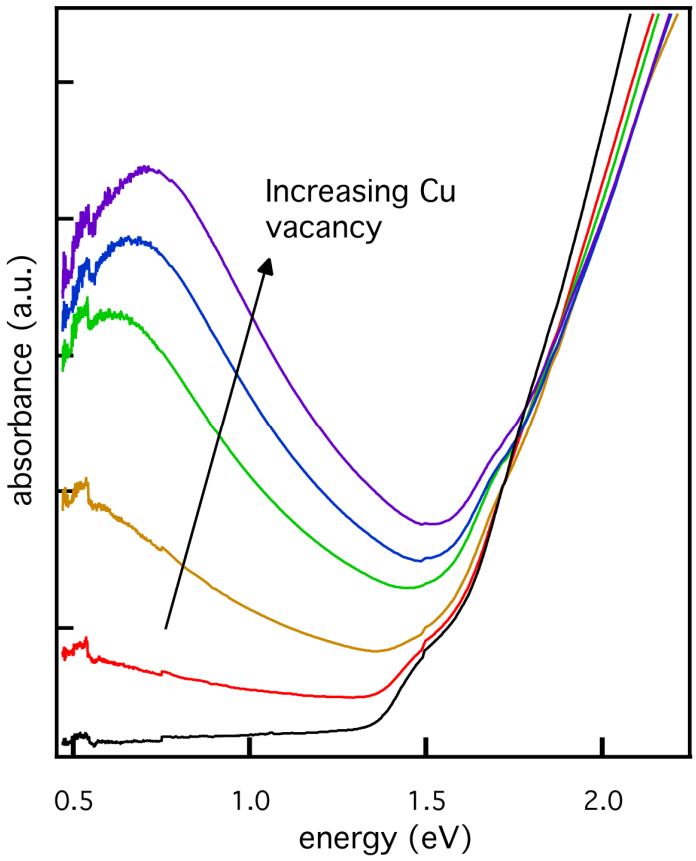

Fig. 4.Active tuning of LSPRs in Cu(I)S nanorods by introduction of copper vacancies. The spectrum of nearly stoichiometric Cu_2S nanorods, shown in black, does not exhibit any NIR LSPR absorbance. On exposure to oxygen (ambient air), copper vacancies are generated resulting in the emergence of a NIR LSPR peak, which increases in intensity and blue-shifts with increasing time of oxygen exposure (red to violet), to an eventual peak position of 0.7 eV. The band-gap absorption onset and exciton peak also blue-shifts from ~1.5 eV to ~1.7 eV with increasing time of oxygen exposure. Similar to gold nanorods, it is possible that Cu(I)S nanorods have an additional LSPR mode due to oscillations along the long-axis. Considering the high aspect ratio of the nanorods (ca. 10), such a mode is expected to be at significantly lower energies (far-IR), out of the range of our spectrometer.

While the nanorods show a band-gap absorption onset and an excitonic feature around 1.5 eV, there is no NIR absorbance indicating the absence of an LSPR mode in the NIR. On exposure to oxygen, which is known to generate copper vacancies in copper

(I) sulfide,[21,28] an LSPR band emerges. The LSPR band progressively increases in intensity and blue-shifts with increasing time of oxygen exposure, which is clearly attributable to an increasing density of generated copper vacancies. This demonstrates that control of the doping density could allow dynamic tuning of the LSPR frequency and possibly even complete ON/OFF switching of the LSPR mode.

The increase in free carrier density due to vacancy formation is also accompanied by a blue-shift of the absorption band onset and exciton peak from ~1.5 eV to ~1.7 eV. It is possible that this is due to a Moss-Burstein effect where the free carriers (holes) resulting from the copper vacancies occupy the top of the Cu(I)S valence band, leading to an increase in the optical band-gap.[28] However, it is also possible that the blue-shift results from the dipolar coupling of the LSPR oscillation with the exciton, similar in principle to an AC Stark effect.

Achieving LSPRs and quantum confined excitons within the same nanostructure opens up a number of other possibilities. Unlike hybrid metallic/semiconductor nanostructures, in this case, energy transfer and synergistic coupling between photonic modes and excitons is not limited by the physicochemical interface between the two components. The LSPR mode, if resonant with excitonic transitions, can enhance i) the absorption cross-section of the excitonic transition *via* an antenna effect, and/or ii) the spontaneous emission rate and the yield *via* the Purcell effect. The plasmonic near-field coupled with the excitonic transitions facilitates non-linear effects such as enhanced two-photon absorption, dynamical Stark shifts, ultrafast optical switching and manipulation of excitonic transitions,[34,35] photonic up-conversion,[3] and sub-wavelength lasing.[36] On the other hand, energy pumped into the excitonic modes can channel into the LSPR mode making possible single quantized plasmon generation.[37]

Materials and Methods

The synthesis of copper (I) sulfide QDs, based on previous work from our group,[18] was adapted here to achieve size control and monodispersity in the range of 2.5 to 6 nm. In two separate round bottom flasks using common air-free Schlenck line techniques, copper and sulfur precursor solutions were formed. QDs were synthesized by introducing the copper precursor solution into the sulfur solution. The copper precursor solution was composed of 1.134 g (4.3 mmol) copper(II)acetylacetonate ($Cu(acac)_2$) and 13 mL (41 mmol) oleic acid heated to 110^{o}C. The sulfur-containing precursor was made from ammonium

diethyldithiocarbamate, 1-dodecanethiol (10 mL), and oleic acid heated to 180^{o}C under argon. A 3-mL portion of the blue copper precursor suspension was withdrawn and added to the second flask. The oleic acid in the sulfur flask was adjusted to have a total reaction volume of 20 mL after the injection. The reaction was allowed to proceed for 3-12 minutes at which time the heat was removed. Control of the QD size was achieved by the variation of the Cu to S precursor ratio (Supplementary Information). The average size and size distribution of the colloids was measured by transmission electron microscopy (TEM) and crystallinity was characterized by electron diffraction (Fig. 2). QDs of 6-nm size were obtained using a Cu:S ratio of 1:1.25. For the smallest sub-3-nm QDs, a ratio of 3:0.63 was used. At the highest Cu:S ratio, a polydisperse mixture of nanospheres and nanoplates was obtained. In addition to the precursor ratio, the growth time was adjusted from 3-12 minutes for small to large QDs. The reaction mixture, following cooling to room temperature, was centrifuged at 4500 rpm to separate the QDs from unreacted precursors. In the case of smaller QDs, a few mL of methanol was added as a non-solvent to aid the separation. The QDs were redispersed in toluene followed by an additional separation step using isopropanol or methanol. The precipitated QDs were dispersed in solvents with high NIR transmission: tetrachloroethylene (TCE), carbon disulfide (CS_2), and carbon tetrachloride (CCl_4) for optical characterization, however they are also soluble in common non-polar solvents such as hexane or toluene.

Visible-NIR region absorbance spectra of the QD colloids were measured in all three solvents on a Shimadzu UV3600 spectrophotometer. X-ray diffraction patterns were collected on a GADDS Hi-Star D8 diffractometer (Bruker) using Co Kα radiation (1.790 Å) and a general area detector. Samples were prepared by deposition of a concentrated solution of QDs on a glass plate followed by drying in air. The patterns were background-subtracted and compared with those published in the Joint Committee of Powder Diffraction Standards (JCPDS) database for bulk monoclinic low chalcocite ((JCPDS# 033-0490)) and djurleite (JCPDS# 034-0660). Transmission electron microscopy images and electron diffraction were acquired on a 200 kV Tecnai G220 S-TWIN with a Gatan SC200 CCD camera. Samples were prepared by drop casting the QD solution on carbon-coated copper grids.

CdS nanorods were synthesized via a hot injection method described before.[33] Cu_2S nanorods were prepared by the room temperature cation exchange of CdS nanorods with Cu^{+}. CdS nanorods (4 mL in hexane; 1.7 mM Cd^{2+}) were stirred vigorously with a methanolic solution of 20x molar (10x stoichiometric excess) of tetrakis(acetonitrile)copper(I) hexafluorophosphate for a few minutes in an oxygen-free environment. Methanol from the biphasic mixture was separated leaving behind the Cu_2S nanorods in hexane. The solution was completely dried with N_2 and dispersed in TCE for Vis-NIR absorbance measurements in an air-tight NIR cuvette. The nanorod solution was exposed to oxygen (in ambient air and room temperature) and a sequence of absorbance spectra were collected in air over a period of ~6 hours.

Acknowledgements

Work on copper sulfide nanocrystal synthesis and optical and structural characterization was supported by the Physical Chemistry of Semiconductor Nanocrystals Program, KC3105, Director, Office of Science, Office of Basic Energy Sciences, of the United States Department of Energy under contract DE-

AC02-05CH11231. Work on LSPR response characterization, chemical tuning, and vacancy density profiling was supported by a Miller Fellowship awarded to P.K.J. We thank Jessy Baker Rivest and Jao van de Lagemaat for discussions and Lam-Kiu Fong for a CdS nanorod sample.

Author Contributions

J.L synthesized copper sulfide quantum dots and performed optical characterization. P.K.J performed work on LSPR characterization and assignment; Cu(I)S crystallography and vacancy profiling; and active chemical tuning of LSPRs. T. E. performed electron microscopy of copper sulfide nanocrystals. J.L., P.K.J., T.E., and A.P.A. discussed results and prepared the manuscript and subsequent revisions.

References

1. Hutter, E. & Fendler, J. Exploitation of Localized Surface Plasmon Resonance. ***Adv Mater*** **16**, 1685-1706 (2004).
2. Jain, P. K., Huang, X., El-Sayed, I. & El-Sayed, M. Noble Metals on the Nanoscale: Optical and Photothermal Properties and Some Applications in Imaging, Sensing, Biology, and Medicine. *Acc. Chem. Res.* **41**, 1578-1586 (2008).
3. Atwater, H. A. & Polman, A. Plasmonics for improved photovoltaic devices. *Nat. Mater.* **9**, 205-213 (2010).
4. Kneipp, K. *et al*. Single Molecule Detection Using Surface-Enhanced Raman Scattering (SERS). *Phys. Rev. Lett.* **78**, 1667 (1997).
5. Willets, K. & Van Duyne, R. Localized Surface Plasmon Resonance Spectroscopy and Sensing. *Annu. Rev. Phys. Chem.* **58**, 267-297 (2007).
6. Alvarez, M. M. *et al*. Optical Absorption Spectra of Nanocrystal Gold Molecules. *J. Phys. Chem. B* **101**, 3706-3712 (1997).
7. Pérez-Juste, J., Pastoriza-Santos, I., Liz-Marzán, L. M. & Mulvaney, P. Gold nanorods: Synthesis, characterization and applications. *Coord. Chem. Rev.* **249**, 1870-1901 (2005).
8. Kanehara, M., Koike, H., Yoshinaga, T. & Teranishi, T. Indium Tin Oxide Nanoparticles with Compositionally Tunable Surface Plasmon Resonance Frequencies in the Near-IR Region. *J. Am. Chem. Soc.* **131**, 17736-17737 (2009).
9. Williams, C. R. *et al*. Highly confined guiding of terahertz surface plasmon polaritons on structured metal surfaces. *Nat Photon* **2**, 175-179 (2008).
10. Kundu, J., Le, F., Nordlander, P. & Halas, N. J. Surface enhanced infrared absorption (SEIRA) spectroscopy on nanoshell aggregate substrates. *Chem. Phys. Lett.* **452**, 115-119 (2008).
11. Norris, D. J., Efros, A. L. & Erwin, S. C. Doped Nanocrystals. *Science* **319**, 1776-1779 (2008).
12. Potter, R. W. An electrochemical investigation of the system copper-sulfur. *Econ. Geol.* **72**, 1524-1542 (1977).
13. Du, X. *et al*. Shape-Controlled Synthesis and Assembly of Copper Sulfide Nanoparticles. *Cryst. Growth Des.* **8**, 2032-2035 (2008).
14. Ghezelbash, A. & Korgel, B. A. Nickel Sulfide and Copper Sulfide Nanocrystal Synthesis and Polymorphism. *Langmuir* **21**, 9451-9456 (2005).
15. Li, S. *et al*. Synthesis and assembly of monodisperse spherical Cu_2S nanocrystals. *J. Colloid Interface Sci.* **330**, 483-487 (2009).
16. Sigman, M. B. *et al*. Solventless Synthesis of Monodisperse Cu2S Nanorods, Nanodisks, and Nanoplatelets. *J. Am. Chem. Soc.* **125**, 16050-16057 (2003).
17. Han, W. *et al*. Synthesis and Shape-Tailoring of Copper Sulfide/Indium Sulfide-Based Nanocrystals. *J. Am. Chem. Soc.* **130**, 13152-13161 (2008).
18. Wu, Y., Wadia, C., Ma, W. L., Sadtler, B. & Alivisatos, A. P. Synthesis and photovoltaic application of copper(I) sulfide nanocrystals. *Nano Lett.* **8**, 2551-2555 (2008).

19. Zhao, Y. *et al*. Plasmonic Cu2S Nanocrystals: Optical and Structural Properties of Copper-Deficient Copper(I) Sulfides. *J. Am. Chem. Soc.* **131**, 4253-4261 (2009).
20. Evans, H. T., Jr. Djurleite ($Cu_{1.94}S$) and Low Chalcocite (Cu_2S): New Crystal Structure Studies. *Science* **203**, 356-358 (1979).
21. Sands, T. D., Washburn, J. & Gronsky, R. High Resolution Observations of Copper Vacancy Ordering in Chalcocite (Cu_2S) and the Transformation to Djurleite ($Cu_{1.97\ to\ 1.94}S$). *Phys. Stat. Sol. (a)* **72**, 551-559 (1982).
22. Tsu, R., Howard, W. E. & Esaki, L. Optical and Electrical Properties and Band Structure of GeTe and SnTe. *Phys. Rev.* **172**, 779 (1968).
23. Mulder, B. J. Optical properties and energy band scheme of cuprous sulphides with ordered and disordered copper ions. *Phys. Stat. Sol. (a)* **18**, 633-638 (1973).
24. Alivisatos, A. P. Semiconductor Clusters, Nanocrystals, and Quantum Dots. *Science* **271**, 933-937 (1996).
25. Luther, J. M., Zheng, H., Sadtler, B. & Alivisatos, A. P. Synthesis of PbS Nanorods and Other Ionic Nanocrystals of Complex Morphology by Sequential Cation Exchange Reactions. *J. Am. Chem. Soc.* **131**, 16851-16857 (2009).
26. Grozdanov, I. & Najdoski, M. Optical and Electrical Properties of Copper Sulfide Films of Variable Composition. *J. Solid State Chem.* **114**, 469-475 (1995).
27. Putnis, A. The transformation behaviour of cuprous sulphides and its application to the efficiency of Cu_xS–CdS solar cells. *Phil. Mag.* **34**, 1083-1086 (1976).
28. Lukashev, P., Lambrecht, W. R. L., Kotani, T. & van Schilfgaarde, M. Electronic and crystal structure of Cu2-x S : Full-potential electronic structure calculations. *Phys. Rev. B* **76**, 195202 (2007).
29. Roseboom, E. H., Jr. Djurleite, Cu1.96S, A new mineral. *Am. Mineralogist* **47**, 1181-1184 (1962).
30. Gurin, V. S. *et al*. Sol–gel silica glasses with nanoparticles of copper selenide: synthesis, optics and structure. *Int. J. Inor. Mater.* **3**, 493-496 (2001).
31. Deka, S. *et al*. Phosphine-Free Synthesis of p-Type Copper(I) Selenide Nanocrystals in Hot Coordinating Solvents. *J. Am. Chem. Soc.* **132**, 8912-8914 (2010).
32. Mansour, B. A., Demian, S. E. & Zayed, H. A. Determination of the effective mass for highly degenerate copper selenide from reflectivity measurements. *J. Mater. Sci. :Mater. Electron.* **3**, 249-252 (1992).
33. Sadtler, B. *et al*. Selective Facet Reactivity during Cation Exchange in Cadmium Sulfide Nanorods. *J. Am. Chem. Soc.* **131**, 5285-5293 (2009).
34. Zhang, J., Tang, Y., Lee, K. & Ouyang, M. Tailoring light-matter-spin interactions in colloidal hetero-nanostructures. *Nature* **466**, 91-95 (2010).
35. Lee, J., Hernandez, P., Lee, J., Govorov, A. O. & Kotov, N. A. Exciton-plasmon interactions in molecular spring assemblies of nanowires and wavelength-based protein detection. *Nat Mater* **6**, 291-295 (2007).
36. Oulton, R. F. *et al*. Plasmon lasers at deep subwavelength scale. *Nature* **461**, 629-632 (2009).
37. Akimov, A. V. *et al*. Generation of single optical plasmons in metallic nanowires coupled to quantum dots. *Nature* **450**, 402-406 (2007).